Recovery of Realistic Polymer Melts after Simple Shear Flows

Ulrik Borgbjerg and Juan J. de Pablo*

Department of Chemical Engineering and Rheology Research Center, University of Wisconsin, Madison, Wisconsin 53706

Received November 9, 1994; Revised Manuscript Received February 21, 1995[⊗]

ABSTRACT: This work examines the constrained recovery of polydisperse polymer melts after steady shear flow. Calculations are performed in the framework of the Curtiss−Bird theory both by conventional numerical integrations and by nonequilibrium Brownian dynamics simulations. The latter approach is shown to have significant advantages. The predicted curves of ultimate recovery versus dimensionless shear rate exhibit unusual maxima; these are compared to experimental data for recovery.

Introduction

This is the second of two papers devoted to the study of the recovery of polymer melts within the framework of the Curtiss−Bird model (CBM). The first paper[1] examined constrained recovery after steady shear flow and free recovery after steady elongational flow for monodisperse polymer melts. This paper discusses polydispersity effects and is limited to the case of recovery after shear flow. Hereafter, we refer to our first paper as 1.

In 1, we presented a stochastic simulation method for calculation of recovery and we compared its results to those of conventional numerical integration techniques. The stochastic method proved to be superior in a number of respects. One of its main advantages was its performance for calculation of viscometric functions at high shear rates.

The dynamic properties of polymer melts in a shear flow depend on the dimensionless shear rate $\lambda\,\dot{\gamma}_0$, where λ is a characteristic time constant that depends on the molecular weight of the polymer. Polymer melts with a high degree of polydispersity exhibit a wide spectrum of characteristic times, thereby leading to a recovery (after shear flow) which occurs over a broad spectrum of times. Conventional numerical techniques are ill-suited for the study of polydisperse melts; while for a given value of $\dot{\gamma}_0$ small-chain molecules (having small λ's) require small integration time steps, long-chain molecules (having large λ's) require integrations over long time intervals. The computational demands of stochastic simulations increase only linearly with the size of the time step (those for numerical integrations increase with the square of the time step); their superiority for the problems addressed in this work is therefore apparent.

In 1 it was shown that the Curtiss-Bird model for monodisperse polymer melts leads to reasonable or plausible predictions for constrained recoil after shear flow and free recovery after elongational flow. Unfortunately, comparisons to experimental data were not presented in 1 because constrained recoil experiments have only been reported for highly polydisperse melts. For shear flows, however, we found that, when plotted versus $\lambda\dot{\gamma}_0$, the ultimate recovery exhibits a maximum at around $\lambda\dot{\gamma}_0 \approx 200$. In contrast, the Doi−Edwards model did not exhibit such a maximum, but it greatly overestimated the amount of recoil. That maximum has raised several questions: Is the maximum physical? For what values of $\lambda\dot{\gamma}_0$ does it occur? Is it also observed in polydisperse melts, or is it only present in monodisperse polymers? These are some of the questions that we try to address in this work.

Another important reason for studying the recovery of polydisperse melts is that, to the best of our knowledge, the only published experiental data for constrained recovery after shear flow are for highly polydisperse samples.[2,3] In this work we try to describe these data by means of stochastic simulations of the Curtiss−Bird model. More generally, it is important to point out that most practical applications of polymers involve polydisperse melts; if the Curtiss−Bird model is to be used for engineering work, it must be examined in the context of polydisperse materials.

In our previous work with monodisperse melts, the link tension coefficient ϵ, which measures the anisotropy of friction forces, was a constant between 0 and 0.5. In this study we also explore the consequences of having ϵ depend on molecular weight.

We begin this paper with a formal description of the flow field under consideration, followed by a brief overview of the model for polydisperse melts and a discussion of the stochastic method employed in our work. Next, we explain the effects of polydispersity and discuss the molecular weight distributions employed here. Finally, we present our predictions for viscometric functions and for the ultimate recovery of polydisperse melts after shear flow, and we compare them to experimental data.

Flow Field

This work is concerned only with the constrained recovery (or recoil) of polydisperse melts after steady shear flows. A recovery experiment comprises two stages. In the first stage the fluid is allowed to reach steady state under a constant shear rate $\dot{\gamma}_0$. The stress is then suddenly removed at time t_0, and the fluid recovers to some previously occupied position. During the recovery, the distance between the walls is fixed and assumed to be small. The velocity field for steady shear flow has components $v_x = \dot{\gamma}_0 y$, $v_y = 0$, and $v_z = 0$, where $\dot{\gamma}_0$ is the shear rate. Note that a linear velocity profile is assumed at all times.

During the second stage of the flow, i.e., during recovery starting at $t = t_0$, the velocity profile is also assumed to be linear. At $t = t_0$ the xy-component of the stress tensor τ_{xy} is set equal to 0;[4,5] the flow field therefore becomes time dependent with velocity components $v_x = \dot{\gamma}(t)\,y$, $v_y = 0$, and $v_z = 0$. Figure 1 shows $\dot{\gamma}$, γ, and τ_{xy} as a function of time for a typical recoil

[⊗] Abstract published in *Advance ACS Abstracts,* May 15, 1995.

0024-9297/95/2228-4540$09.00/0

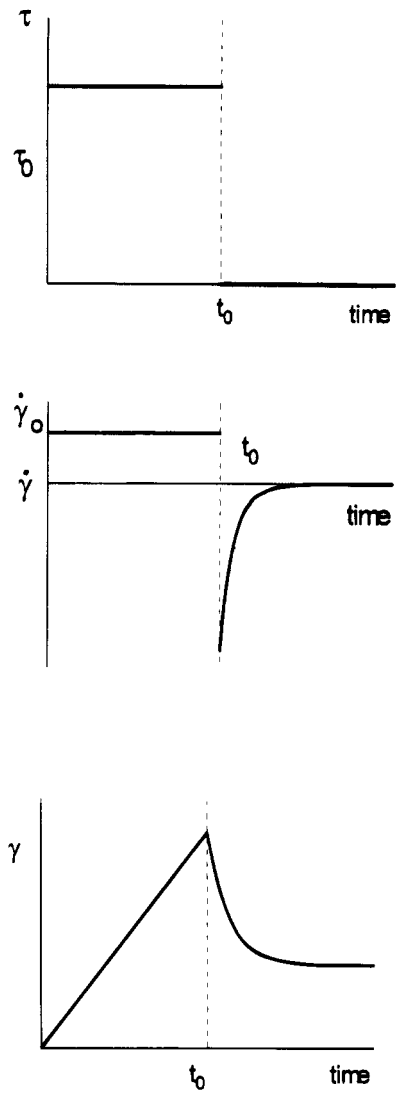

Figure 1. Schematic representation of $\dot{\gamma}$, γ, and τ_{xy} during a recoil calculation.[4]

calculation. The ultimate recovery after shear flow is calculated from

$$\gamma_\infty = \lim_{t\to\infty} \gamma_r(t) \tag{1}$$

where

$$\gamma_r(t) = \int_{t=t_0}^{t} \dot{\gamma}(t')\, dt' \tag{2}$$

The Curtiss–Bird Model

The Curtiss–Bird model (CBM) is based on a kinetic-theory development for an undiluted polymer, in which the molecules are modeled as Kramers' freely jointed bead–rod chains. A polymer molecule of species α is therefore described by N_α massless beads joined by $N_\alpha - 1$ freely rotating rigid links of length a.[6] For a pure polydisperse polymer melt, chains of different species differ only in their number of beads.

The theory of Curtiss and Bird involves four major approximations.[6] The first of these is the *short-range-force approximation*, which states that only beads very close to each other interact. The second is the use of an *anisotropic Stokes' law*, which is an empirical, three-parameter equation for the hydrodynamic drag on a bead. One of the parameters in this law is the *link tension coefficient*, ϵ, which determines the anisotropy of the friction tensor. For $\epsilon = 1$ the tensor is isotropic, and for $\epsilon = 0$ there is no difference between the forces acting on two succeeding beads in the direction of the link joining them. The constitutive equation for monodisperse polymer melts of Curtiss and Bird reduces to that of Doi and Edwards for $\epsilon = 0$. The third approximation, known as the *anisotropic Brownian motion approximation*, states that, on average, the velocity of a bead relative to the center-of-mass velocity is in the direction of the chain. The polymer is therefore said to "reptate" through the melt. The fourth simplification, known as the *mild curvature approximation*, assumes that the chain approximates a curve with continuous derivatives (i.e., with no "kinks").

These approximations result in the following diffusion equation for the single-link probability density function $f_\alpha(\mathbf{u},s,t)$ for species α

$$\frac{\partial f_\alpha}{\partial t} = \frac{1}{\lambda_\alpha}\frac{\partial^2 f_\alpha}{\partial s^2} - \frac{\partial}{\partial \mathbf{u}}\cdot[\kappa\cdot\mathbf{u} - \kappa:\mathbf{uuu}]f_\alpha \tag{3}$$

where $f_\alpha(\mathbf{u},s,t)$ is the time-dependent probability of finding a link of species α at position s along the chain having orientation $\mathbf{u}$. By definition, s is a variable going from 0 to 1, and $\mathbf{u}$ is a unit vector. The time-dependent transposed velocity gradient tensor is denoted by κ, and λ_α is a characteristic time constant for chains of species α. Note that, besides the dependence of the distribution function, the first term in eq 3 depends on the polymer properties and the second term depends only on the flow field. The time constant λ_α is defined as:

$$\lambda_\alpha = \frac{N_\alpha{}^2 \bar{N}^{1+\beta}\zeta a^2}{2k_B T} \tag{4}$$

where k_B is Boltzmann's constant, T is the temperature, N_α is the number of beads of species α, and $\bar{N}$ is the number average of N_α. The friction coefficient ζ, and the chain constraint exponent β are adjustable parameters from the anisotropic Stokes' law. Throughout this work β has been set equal to 0. According to eq 4, λ_α scales as $\lambda_\alpha \sim N_\alpha{}^2\bar{N}$.

The single-link distribution functions $f_\alpha(\mathbf{u},s,t)$ are presumed to obey the following boundary conditions:

$$f_\alpha(\mathbf{u},0,t) - f_\alpha(\mathbf{u},1,t) = \frac{1}{4\pi} \tag{5}$$

From a physical point of view, these conditions ensure that the ends of the chain are oriented randomly.

Having developed expressions for the single-link distribution function, Curtiss and Bird[6] determine the stress tensor $\boldsymbol{\tau}$ according to

$$\boldsymbol{\tau} = k_B T \sum_\alpha n_\alpha N_\alpha \left[\frac{1}{3}\boldsymbol{\delta} - \langle\mathbf{uu}\rangle_\alpha - \lambda_\alpha \epsilon_\alpha \kappa:\langle s(1-s)\mathbf{uuuu}\rangle_\alpha\right] \tag{6}$$

where n_α is the number density of beads for species α, ϵ_α is the link tension coefficient for chains of species α, and $\boldsymbol{\delta}$ is the unit tensor. For simplicity, in the remainder of this work the product $k_B T$ is set to unity. The brackets denote averages with respect to the probability function $f_\alpha(\mathbf{u},s,t)$, e.g.

$$\langle s(1-s)\mathbf{uuuu}\rangle = \int\int f_\alpha(u,s,t)\, s(1-s)\mathbf{uuuu}\, ds\, d\mathbf{u} \tag{7a}$$

and

$$\langle \mathbf{uu}\rangle_\alpha = \int\int f_\alpha(u,s,t)\, \mathbf{uu}\, ds\, d\mathbf{u} \tag{7b}$$

The zero-shear rate viscosity for the polydisperse Curtiss–Bird theory scales in the following manner with the weight-average molecular weight:[6]

$$\eta_0 = CM_w^{3+\beta} \tag{8}$$

where the prefactor C embodies several physical constants and, in general, depends on polymer properties.

One additional new feature of our work is that we allow ϵ to depend on molecular weight. In their original derivation of the model, Curtiss and Bird assumed that ϵ is constant. As mentioned earlier, the link tension coefficient measures the anisotropy of friction forces. For long chains such forces are indeed expected to be highly anisotropic, but for short chains friction forces can become nearly isotropic. For a polydisperse melt it therefore appears reasonable to make ϵ a function of molecular weight. For simplicity we use $\epsilon_\alpha \sim N_\alpha^{-1}$, where subscript α is again used to denote the species. Note, however, that theoretical arguments in favor of a N^{-1} dependence for ϵ have been given in the past.[15]

Molecular Weight Distribution

The polydisperse version of the Curtiss–Bird model (CBM) requires a distinct distribution function $f_\alpha(t,s,\mathbf{u})$ for each species of a mixture. Similarly, the stress tensor is obtained by a sum of contributions over all species. In this work we describe polydisperse melts using a discrete sum over pseudocomponents, although they could also be treated using a continuous approach.[7,8] In our stochastic simulations each species is handled independently. The problem is therefore that of discretizing a given molecular weight distribution and then generating trajectories for each species independently.

For linear polymers, we have only found two sets of experimental data for constrained recoil after shear flow.[2,3] The shear rates examined by Laun and Meissner[2] correspond almost exclusively to the linear regime. Laun[3] has presented experimental data for polyethylene melts over a more extensive range of shear rates; we have decided to model Laun's data because, in addition to the linear region, it also comprises the shear-thinning regime.

Unfortunately, Laun reports only the weight-average molecular weight (98 000) and the number-average molecular weight (9700) of the samples used for his experiments. The details concerning the molecular weight distribution are not provided. We have assumed that these data can be described in terms of a log normal distribution (Figure 2). Our choice is based on the large polydispersity value of Laun's samples = 10.1 and the rather slow rate at which shear thinning is attained (several decades of shear rate without ever reaching a power law region), which is indicative of the presence of very long chains.[7] However, it must be emphasized that this is a major assumption and that further information about the MWD would lead to more meaningful comparisons with experiment.

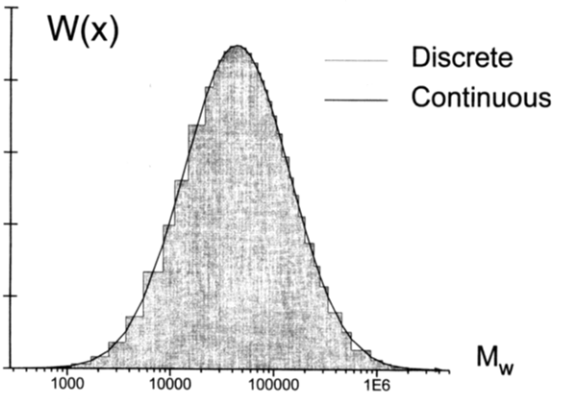

Figure 2. Discretization of the log normal molecular weight distribution. The curve is modeled using 40 pseudocomponents.

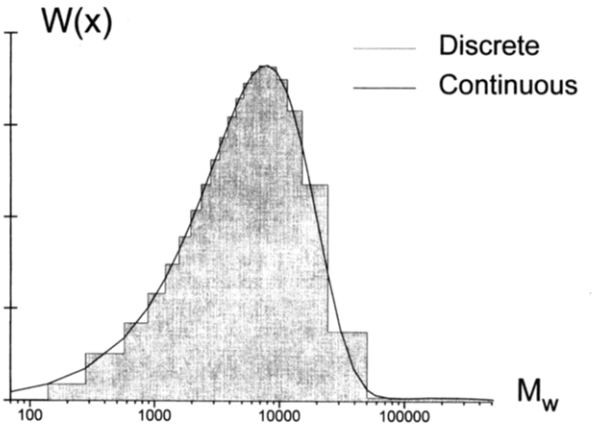

Figure 3. Discretization of the two-most-probable molecular weight distribution. The curve is modeled using 32 pseudocomponents.

We have also considered a sum of two-most-probable-distribution[16] (TMPD) model to describe Laun's data. Figure 3 shows such a distribution. Note, however, that for a given average molecular weight and a given polydispersity the TMPD function contains a smaller number of very long chains than the equivalent log normal distribution function. The onset of shear thinning occurs over a narrower range of shear rates than that for the log normal distribution.

Stochastic Simulations

The stochastic simulation method employed in our work has been described in detail in 1. Here we limit our discussion to pointing out that it relies on the transformation of the Curtiss–Bird diffusion equation for the distribution function (3) into a set of stochastic differential equations for each species of the melt.[9,10] For species α these equations are given by

$$\begin{cases} d\mathbf{u}_\alpha = [\kappa\cdot\mathbf{u} - \kappa:\mathbf{uuu}]_\alpha\, dt & \text{(9a)} \\ ds_\alpha = \sqrt{2/\lambda_\alpha}\, dW & \text{(9b)} \end{cases}$$

where W is a Wiener process. Equations 9 simplify into a pair of stochastic processes for each component in the system: a unidimensional process s and a three-dimensional process $\mathbf{u}$. For a given species α, the only coupling between s and $\mathbf{u}$ occurs through the boundary conditions.

As described in 1, care must be exercised when discretizing eqs 9 for numerical solution. The normalization of $\mathbf{u}$ must be preserved. It is also important to point out that s is reflected whenever it reaches 0 or

1. Furthermore, when a reflection occurs, **u** is chosen randomly on a unit sphere; otherwise, **u** evolves independently of s.

The discretizaton of eqs 9 results in the following equations for s and **u**

$$s_{\alpha,i+1} = s_{\alpha,i} + \left(\frac{2}{\lambda_\alpha}\Delta t\right)^{1/2} W_i \tag{10a}$$

$$\mathbf{u}_{\alpha,i+1} = \mathbf{u}_{\alpha,i} + [\kappa\cdot\mathbf{u} - \kappa:\mathbf{uuu}]_{\alpha,i}\Delta t \approx \frac{\mathbf{u}_{\alpha,i} + [\kappa\cdot\mathbf{u} - \kappa:\mathbf{uuu}]_{\alpha,i}\Delta t}{|\mathbf{u}_{\alpha,i} + [\kappa\cdot\mathbf{u} - \kappa:\mathbf{uuu}]_{\alpha,i}\Delta t|} \tag{10b}$$

where the W_i's are independent random numbers generated from a Gaussian distribution with unit variance and zero mean. Since s is a Wiener process, it can be reflected back into the interval [0,1] whenever it reaches 0 or 1 during a time step,[11,12] i.e., $s_{r,i+1} = 2B - s_{i+1}$, where B is either 0 or 1 depending on the boundary. The normalization of **u** guarantees that its norm will be preserved.

A steady-state shear flow is first established for a constant shear rate $\dot\gamma_0$. During this stage, the xy-component of the stress tensor is found from eq 6, i.e.

$$\tau_{xy} = -k_B T\sum_\alpha n_\alpha N_\alpha[\langle u_x u_y\rangle_\alpha + \lambda_\alpha\epsilon_\alpha\dot\gamma_0\langle s(1-s)u_x^2 u_y^2\rangle_\alpha] \tag{11}$$

Once τ_{xy} has reached its steady-state value, the recoil experiment can begin. As indicated above, the shear rate $\dot\gamma(t)$ is now a function of time, but the xy-component of the stress tensor is constant and set equal to 0. The shear rate is therefore calculated at each time step according to

$$\dot\gamma(t) = -\frac{\sum_\alpha n_\alpha N_\alpha\langle u_x u_y\rangle_\alpha}{\sum_\alpha n_\alpha N_\alpha\lambda_\alpha\epsilon_\alpha\langle s(1-s)u_x^2 u_y^2\rangle_\alpha} \tag{12}$$

Once $\dot\gamma(t)$ is known, the ultimate recoil can be calculated using eq 1.

When performing stochastic simulations according to eqs 10, several technicalities must be observed. These have been discussed in 1 and need not be given again. Here we only point out that the probability for overseen reflections during the $(i+1)$th time step is calculated from

$$P = e^{-(\lambda/\Delta t)(B-s_i)(B-s_{i+1})} \tag{13}$$

where B is either 0 or 1, depending on which boundary is the nearest.[13] A random number R is then generated uniformly between 0 and 1; if $P > R$, an overseen reflection is assumed to have occurred; if $P < R$, it is assumed that no overseen reflections took place.

As in 1, when an overseen reflection occurs (i.e., if $P > R$), or also when a real reflection occurs, in which case $s_{i+1} \notin [0,1]$, the last reflection time is determined by a bisection procedure (see Appendix A in 1). With such a procedure, the stochastic algorithm leads to errors of order Δt.[14] To estimate the value of the ultimate recoil in the limit of zero time step, we conduct several simulations for the same conditions but using different time steps and we extrapolate to zero time step by means of a linear regression.

Conventional Numerical Method

For the sake of completeness, in this work we also compare the results of our stochastic simulations to those of conventional numerical integration techniques. The procedure we follow here to solve the recoil problem numerically has also been described earlier;[1] in this paper we only outline the equations that must be solved.

The xy-component of the stress tensor is determined according to[6]

$$\tau_{xy} = -k_B T\sum_\alpha n_\alpha N_\alpha[\int_{-\infty}^t \mu_\alpha(t-t')\,A_{xy}^{(2)}|_\Gamma\,dt' + \epsilon_\alpha\lambda_\alpha\int_{-\infty}^t \nu_\alpha(t-t')\,B_{xy}^{(2)}|_\Gamma\,dt'] \tag{14}$$

where the "memory" functions μ_α and ν_α are given by

$$\mu_\alpha(t-t') = \frac{8}{\lambda_\alpha}\sum_{n,\text{odd}} e^{-\pi^2 n^2(t-t')/\lambda_\alpha} \tag{15a}$$

$$\nu_\alpha(t-t') = \frac{16}{\pi^2\lambda_\alpha}\sum_{n,\text{odd}} n^{-2} e^{-\pi^2 n^2(t-t')/\lambda_\alpha} \tag{15b}$$

and where

$$A_{xy}^{(2)} = \frac{1}{2\Gamma}\int_0^1[1 + g^{-1}(\Gamma^2 x^2 - 1)]\,dx \tag{16a}$$

$$B_{xy}^{(2)} = \frac{\dot\gamma_{xy}}{4\Gamma^2}\int_0^1\{1 + g^{-3}[(3\Gamma^6 + 8\Gamma^4)x^6 - (7\Gamma^4 + 8\Gamma^2)x^4 + 5\Gamma^2 x^2 - 1]\}\,dx \tag{16b}$$

with

$$g = [(\Gamma^4 + 4\Gamma^2)x^4 - 2\Gamma^2 x^2 + 1]^{1/2} \tag{17}$$

and

$$\Gamma(t,t') = -\gamma_{xy}(t,t') = \int_{t'}^t \dot\gamma_{xy}(t'')\,dt'' \tag{18}$$

The recovery problem is solved by setting the left-hand side of eq 14 equal to zero and then solving for $\dot\gamma(t)$, which enters that equation explicitly through $B_{xy}^{(2)}$ (eq 16b). Note that $\dot\gamma(t)$ also enters the stress tensor implicitly through the dependence of $A_{xy}^{(2)}$ and $B_{xy}^{(2)}$ on Γ (eq 18). A predictor–corrector scheme is employed to handle this implicit dependence. A Romberg integration scheme is used to evaluate the memory integrals in eq 14.

Results and Discussion

We begin this section by comparing the resuls of stochastic simulations to those of conventional numerical-integration techniques. The two systems for which comparisons are made consist of a fictitious binary blend of low molecular weight chains and high molecular weight chains. For both systems the weight fraction of each of the two components is 0.5. The ratios of the two molecular weights are 10 and 38, respectively. The corresponding characteristic time constants for the short and long species are therefore chosen to be 1 and 100, and 1 and 1444, respectively. This large difference in

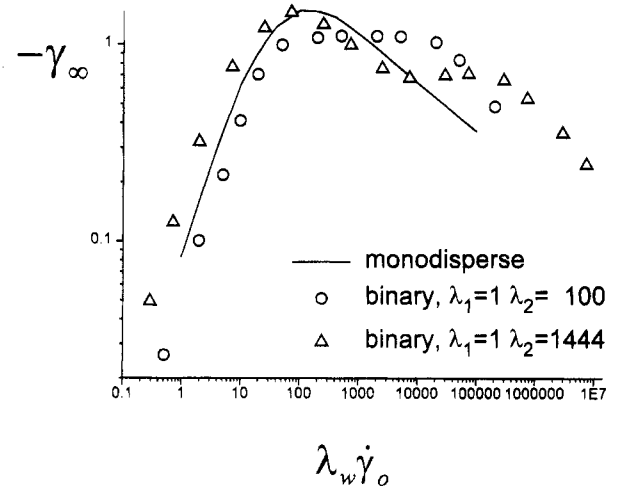

Figure 4. Recovery curve for a monodisperse melt (solid line) and two fictitious binary blends. One blend contains species which have a characteristic time of unity and of 100. The other blend contains species which have a characteristic time of unity and of 1444, respectively. The weight fraction is 0.5 for the two components in both blends.

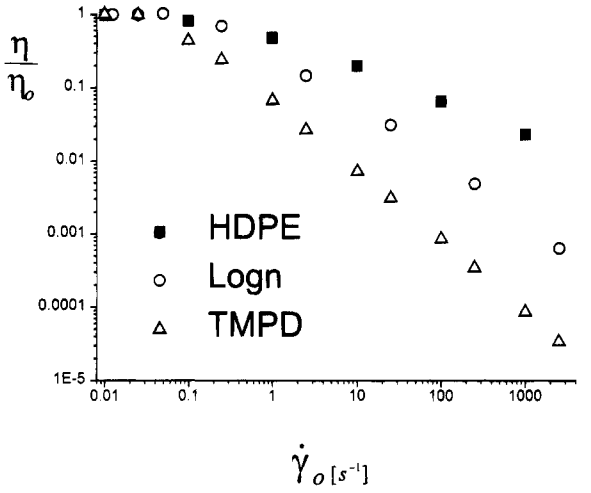

Figure 5. Viscosity for the high-density polyethylene melt (HDPE). The solid squares show experimental data.[3] The open circles show results of stochastic simulations for a log normal molecular weight distribution function with constant link tension coefficient $\epsilon = 0.3$. The open triangles show results of stochastic simulations for a "two-most-probable-distribution" model (TMPD).

λ's complicates significantly the numerical solution of the relevant equations, especially in the latter case. This is why only simple binary blends are examined using conventional numerical methods.

Figure 4 shows the ultimate recovery for these two blends as a function of shear rate. When these recovery curves are compared to that for a monodisperse melt, the biggest difference is seen in the shape of the maximum. When the two λ's are separated, the maximum is first stretched out over a wider range of shear rates and it eventually splits up into two maxima. For monodisperse melts, the maximum recovery only extends over less than a decade of shear rates. For the two binary blends the maximum extends over several decades of shear rate. We believe that each of the two species is responsible for a maximum; when their time constants are different enough, the corresponding maxima separate and appear as two distinct peaks on the recovery curve. If the λ's are not too different, the maximum is only stretched.

Next we compare the resuls of our calculations to experimental data. For our stochastic simulations we dicretize the molecular weight distribution (MWD) into 40 pseudocomponents; Figures 2 and 3 illustrate how the discretization is carried out. In the simulations, each pseudocomponent has an individual single-link distribution function described by an individual stochastic process. When calculating the stress tensor, however, these individual processes are weighted according to the area of the corresponding "bar" in Figures 2 and 3. Depending on the shear rate, we used 1000–5000 trajectories to simulate the averages coresponding to each individual species. Note that stresses in the fluid are highly sensitive to contributions from high molecular weight components. To get a better resolution of such contributions, we use more trajectories for the very high molecular weight components. The recovery calculations therefore required a total of 40×10^3 to 200×10^3 trajectories.

In order to compare our recoil calculations to experimental data for high-density polyethylene melts, we first need to scale our results by a suitable time constant. Following Schieber,[17] this time constant is determined by shifting the scaled viscosity function along the $\dot{\gamma}$-axis until the best description of the data is achieved. It is important to emphasize that the Curtiss–Bird model predicts that as $\dot{\gamma}_0 \to \infty$ the viscosity scales as the inverse shear rate. Experimental data, however, suggest that the viscosity scales with a lower exponent of the shear rate. We therefore adjust λ so that a good description of the viscosity data is obtained in the low-to-intermediate shear rate regime.

Figure 5 shows our results for viscosity for constant $\epsilon = 0.3$. This value of ϵ was selected because previous comparisons of the Curtiss–Bird model and experiments suggest that this is a reasonable choice.[6] The filled squares represent experimental data for a high-density polyethylene melt (HDPE) by Laun.[3] The open circles show results of stochastic simulations for a log normal distribution (Figure 2) with a constant link tension coefficient. The open triangles show results of stochastic simulations for a two-most-probable-distribution model (TMPD) (Figure 3). As can be seen in Figure 5, for the TMPD model the onset of shear-thinning behavior occurs over a narrow range of shear rates. This fast onset of a power-law behavior is attributed to a lack of very long chains in the TMPD model. The log normal molecular weight distribution has a longer tail and gives results for viscosity that are closer to the corresponding experimental values.

Note, however, that agreement with experiment is not as good for Laun's samples of HDPE as it was for the polymeric systems investigated by Schieber. Since the largest polydispersity studied by Schieber was 3.8 and since that of Laun's HDPE was 10.1, it is difficult to make comparisons between his and our work.

Values of λ obtained from viscosity data were subsequently used to examine recovery. Parts a and b of Figure 6 show the time-dependent shear rate during recovery for $\lambda\dot{\gamma}_0 = 0.01$ and for $\lambda\dot{\gamma}_0 = 10$, respectively. The simulated shear rates exhibit large fluctuations about their average value, particularly as equilibrium is approached. These curves are described fairly accurately by the sum of two exponentials, indicating the sharp separation of characteristic time constants (between short and long chains) that govern the recovery process at different times.

Figure 7 shows results of stochastic simulations (for a constant value of ϵ) and experimental data for recovery

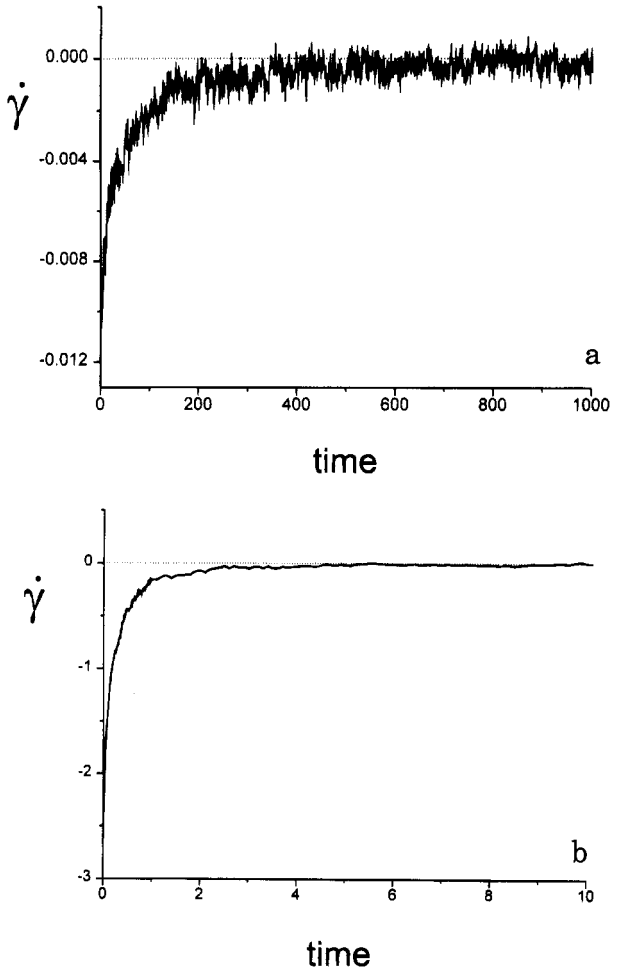

Figure 6. (a) Shear rate $\dot{\gamma}(t)$ during constrained recovery after shear flow. The line shows results of a stochastic simulation of 10^5 trajectories for $\lambda\dot{\gamma}_0 = 0.01$ and $\epsilon = 0.3$. (b) Shear rate $\dot{\gamma}(t)$ during constrained recovery after shear flow. The line shows results of a stochastic simulation of 10^5 trajectories for $\lambda\dot{\gamma}_0 = 10$ and $\epsilon = 0.3$.

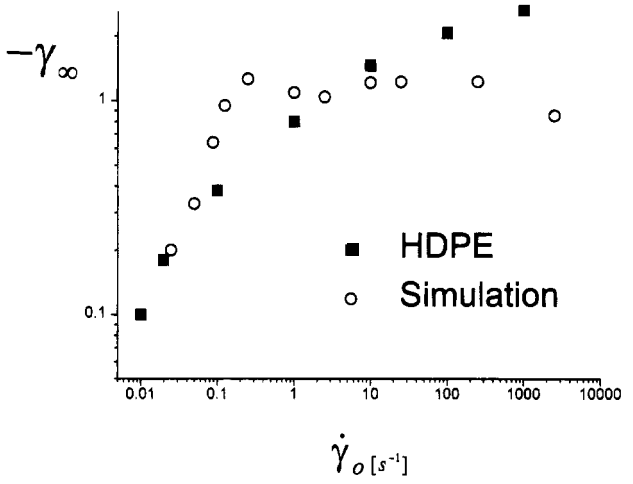

Figure 7. Recovery for a high-density polyethylene melt (HDPE). The solid squares show experimental data.[3] The open circles are from stochastic simulations based on a log normal molecular weight distribution function and a constant value of the link tension coefficient $\epsilon = 0.3$.

as a function of shear rate. The simulations predict two maxima in the recovery curve. These maxima are not observed in the experimental data. They are, however, consistent with our results for a simple binary blend (Figure 4). This bindary blend actually has the same

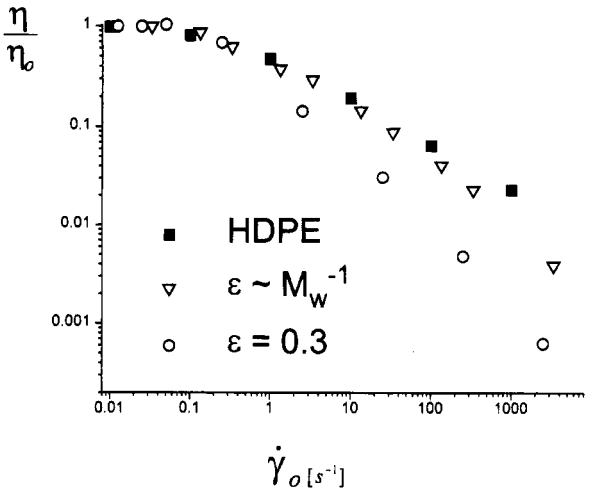

Figure 8. Viscosity for a high-density polyethylene melt (HDPE). The solid squares show experimental data.[3] The open symbols show results of stochastic simulations with a log normal molecular weight distribution function. The open circles correspond to a constant value of the link tension coefficient $\epsilon = 0.3$. The open triangles correspond to a molecular-weight-dependent ϵ ($\sim M_w^{-1}$) with $\epsilon \in [0.05,0.5]$.

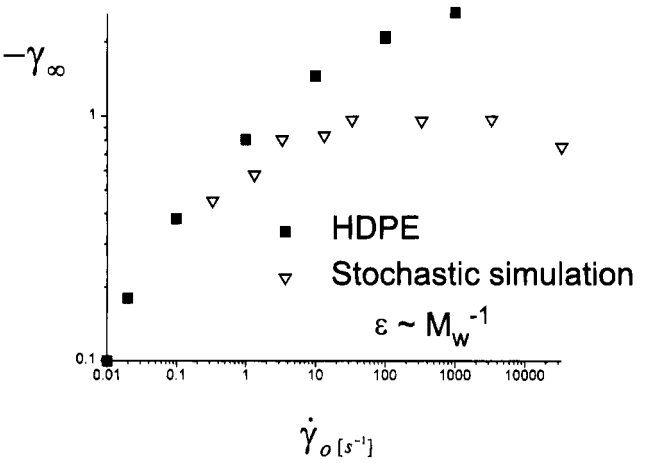

Figure 9. Recovery for a high-density polyethylene melt (HDPE). The solid squares show experimental data.[3] The open triangles show results of stochastic simulations with a log normal molecular weight distribution function and a molecular-weight-dependent ϵ ($\sim M_w^{-1}$).

polydispersity value as Laun's data. Note, however, that the values of recovery at low shear rates are predicted quantitatively by the theory.

For the log normal distribution we also performed simulations with a molecular-weight-dependent ϵ. We let ϵ_α scale as N_α^{-1}, where α denotes the species; our choice of $\epsilon_\alpha \in [0.05, 0.5]$ is based on experiments[6] and our own experience. Except for the changes in ϵ_α, the simulations with the log normal distribution are identical to those shown in Figures 5 and 7. Figure 8 shows viscosity curves for Laun's data (filled squares), for the simulation with the log normal distribution with constant ϵ (open circles), and for the simulation with a molecular-weight-dependent ϵ (open triangles). The onset of the power-law behavior is delayed when a variable ϵ_α is employed and good agreement with experiment is obtained. Figure 9 shows the result of stochastic simulations (for ϵ_α scaling as N_α^{-1}) and experimental data for recovery as a function of shear rate. In this case only one maximum is observed. The agreement with experiment is satisfactory in the linear

regime. However, the results deviate from experiment at high shear rates.

At this point we must emphasize that our resuls for recovery are highly sensitive to the details of the molecular weight distribution function. We have assumed that the samples used in the experiments can be interpreted by a log normal distribution, but this might not be the case. We must also stress that simulations for polydisperse systems are delicate, particularly in the vicinity of the linear viscoelastic regime, and therefore require significant amounts of computer time.

However, in spite of our assumptions regarding the particular form of the distribution function, the Curtiss–Bird model is able to capture the main characteristics of the recovery of polydisperse melts after shear flows. The predictions reported here have been carried out by using time constants determined from steady-state viscosity data; these constants have not been readjusted to describe the recoil data. For low-to-moderate shear rates the ultimate recovery is predicted with reasonable accuracy. For high shear rates it predicts the right trends and the right orders of magnitude. It is conceivable that other molecular weight distributions would lead to semiquantitative results for recovery.

Conclusions

We have used the Curtiss–Bird model (CBM) to calculate the recovery after steady shear flow for polydisperse melts. We have examined an idealized binary melt and a more realistic polydisperse melt having a broad distribution of molecular weights.

Our calculations for binary blends were carried out by means of conventional numerical techniques and by stochastic simulations. Both approaches lead to identical results, but stochastic simulations were found to be more efficient, particularly for systems that exhibit a broad spectrum of characteristic times.

For polydisperse melts, we found that the recovery curve corresponding to a constant link tension coefficient exhibits two maxima when plotted as a function of shear rate. These maxima are not observed in the available experimental data. In the absence of more specific information regarding the details of the molecular weight distribution used for the recovery experiment, it is difficult to draw additional conclusions. Clearly, there is a need for experimental recovery data on well-characterized samples. It is also important to mention that throughout this work we have assumed that a linear velocity profile is established from the beginning of the recovery experiment. The consequences of assuming a linear velocity profile at all times are being examined by means of combined stochastic/spectral simulations, the results of which will be presented in the future.[18]

For molecular-weight-dependent link tension coefficients, ϵ_α, very good agreement was observed between calculated and experimental viscosities. In that case only one maximum was observed in the recovery curve. Agreement with experiment was good in the linear regime, but it deteriorated at higher shear rates. Again, the discrepancies between experiment and simulation could be explained by an inappropriate choice of the molecular weight distribution function; overall, the predictions of the Curtiss–Bird theory are consistent with experiment. The right trends and the right orders of magnitude are obtained for the recovery of realistic polydisperse melts after cessation of shear flow.

Finally, we must emphasize that stochastic simulations in the vicinity of the linear viscoelastic regime are delicate and require exensive computations. There is a clear need to refine or improve the stochastic methods that we have employed in this work. Improved methods will lead to more accurate results and will increase our ability to address larger scale problems.

Acknowledgment. The authors are grateful to Hans Christian Öttinger for helpful discussions. This work was supported in part by the National Science Foundation. J.J.dP. is also grateful to the Camille and Henry Dreyfus Foundation for a New Faculty Award and to the donors of the Petroleum Research Fund, administered by the American Chemical Society. Most of the calculations performed in this work were performed on an IBM580 workstation awarded to the authors by the IBM Corp. under the SUR (Sheared University Research) program.

Appendix

A reflection can arise in two different ways during a given time step. If $s_{i+1} \notin [0,1]$, the reflection was observed. If $s_{i+1} \in [0,1]$ but $P > R$, then an overseen reflection took place. In both cases the last reflection time $t_r \in [t,t+\Delta t]$ is determined by a bisection procedure; a time step is then taken for $\mathbf{u}$ (starting from a random value) over the remainder of the original time step, i.e., from t_r to $t + \Delta t$. In what follows we describe the bisection method. Note that the accuracy of the stochastic integration scheme will still be of order Δt. However, the extrapolation to zero time step will be facilitated significantly by reducing the prefactor of the time-step dependence.

Both observed and overseen reflections can be treated on the same basis by taking advantage of the reflection principle of the Wiener process and reflecting s_{i+1} over the boundary in the case of an overseen reflection.[17,18]

At time t, $s_i \in [0,1]$, and $s_{i+1} \notin [0,1]$ at time $t + \Delta t$. This is a Wiener process, bounded at both ends; s must necessarily cross the boundary B at least once during this time step. The bisection method is used to "decide" whether the last boundary crossing occurred in the first or in the last half of the time step. To do so, we calculate $s_{i+(1/2)} = (s_{i+1} + s_i)/2 + 1/2\ (2\Delta t/\lambda)^{1/2}\mathbf{W}_i$ at time $t + (1/2)\Delta t$.[17]

There are now two possibilities, namely, $s_{i+(1/2)} \in [0,1]$ or $s_{i+(1/2)} \notin [0,1]$. If $s_{i+1/2} \in [0,1]$, then a crossing occurred between $t + (1/2)\Delta t$ and $t + \Delta t$; the bisection is therefore continued on the second half of the interval. In the second case, a crossing did occur in the first half of the interval, but one or more additional boundary crossings might also have occurred in the second interval. To decide whether this is the case or not, eq 20 is used with $(1/2)\Delta t$ instead of Δt and $s_{i+(1/2)}$ instead of s_i. If P is larger than a random number, then a crossing did occur; otherwise, no crossings occurred.

This entire procedure can now be repeated until the desired precision is achieved. We used four bisection steps throughout our work.

An obvious way of improving the bisection method as described above would be to find the distribution function for the last crossover time, given the aforementioned double-bounded Wiener process. This function can be found from the distribution of the first crossover time, which could be derived from knowledge of the Wiener process.

References and Notes

(1) Borgbjerg, U.; de Pablo, J. J.; Öttinger, H. C. *J. Chem. Phys.* **1994**, *101*, 7144.
(2) Laun, H. M.; Meissner, J. *Rheol. Acta* **1980**, *19*, 60–67.
(3) Laun, H. M. *Rheol. Acta* **1982**, *21*, 464–469.
(4) Bird, R. B.; Hassager, O.; Armstrong, R. C. *Dynamics of Polymer Liquids*; John Wiley & Sons: New York, 1987; Vol. 1.
(5) Lodge, A. *Elastic Liquids*; Academic Press: New York, 1964.
(6) Bird, R. B.; Curtiss, C. F.; Hassager, O.; Armstrong, R. C. *Dynamics of Polymer Liquids*; John Wiley & Sons: New York, 1987; Vol. 2.
(7) Schieber, J. S.; Curtiss, C. F.; Bird, R. B. *Ind. Eng. Chem. Fundam.* **1986**, *25*, 471–475.
(8) Schieber, J. S. *J. Chem. Phys.* **1987**, *87*, 4917–4927.
(9) Gardiner, C. W. *Handbook of Stochastic Methods*; Springer-Verlag: Berlin, 1990.
(10) Kloeden, P. E.; Platen, E. *Numerical Solutions to Stochastic Differential Equations*; Springer-Verlag: Berlin, 1992.
(11) Hoel, P. G.; Port, S. C.; Stone, C. J. *An Introduction to Stochastic Processes*; Houghton Mifflin: Boston, 1972.
(12) Karlin, S.; Taylor, H. M. *A First Course in Stochastic Processes*, 3rd ed.; Academic Press: New York, 1975; Vol. 2.
(13) Strittmatter, W. *J. Stat. Phys.*, submitted for publication.
(14) Öttinger, H. C. Presentation at the 198th ACS National Meeting, Miami Beach, FL, 1989; preprint.
(15) Öttinger, H. C. *J. Chem. Phys.* **1989**, *92*, 4540–4547.
(16) Peebles, L. H. *Molecular Weight Distributions*; Wiley: New York, 1971.
(17) Schieber, J. S. *J. Chem. Phys.* **1987**, *87*, 4928–4936.
(18) Nyland, G.; de Pablo, J. J.; Graham, M. C. to be submitted for publication.

MA9462464